Available online at www.sciencedirect.com

SciVerse ScienceDirect

Ceramics International 39 (2013) S287–S292

CERAMICS INTERNATIONAL

www.elsevier.com/locate/ceramint

# First principles study on oxygen vacancy formation in rock salt-type oxides MO (M: Mg, Ca, Sr and Ba)

Takashi Yamamoto, Teruyasu Mizoguchi*

*Institute of Industrial Science, University of Tokyo, Tokyo 153-8505, Japan*

Available online 16 October 2012

**Abstract**

Oxygen vacancy formation energies in rock salt-type oxides MO (M: Mg, Ca, Sr, and Ba) were investigated using a first-principles projector augmented wave method based on a density functional theory. Finite-size cell interactions were corrected by calculating with several sizes of the supercells up to 512 atoms, and a band gap correction for a neutral oxygen vacancy was also performed. It was commonly found that the vacancy state induced by the oxygen vacancy is placed below the conduction band minimum (CBM) in all compounds. The position of the vacancy state is deep in MgO and becomes closer to CBM in CaO, SrO, and BaO in that order. By analyzing the oxygen chemical potential dependence, it was found that the formation of oxygen vacancy is preferable under the reduction atmosphere in all compounds. In addition, it was also found that the oxygen vacancy formation energies in MgO, CaO, and SrO are similar to each other, whereas BaO shows lower formation energy than others, indicating that the oxygen vacancy is more abundant in BaO as compared with other rock salt-type oxides. The reason for the lower oxygen vacancy formation energy in BaO is discussed.


*Keywords:* B. Defects; D. Alkaline earth oxides; D. MgO; E. Insulators

## 1. Introduction

Rock salt-type oxide is usually composed of oxygen and divalent cation (M), and a number of rock salt-type oxides have been studied for numerous applications. For instance, MgO is a typical rock salt-type oxide, and it has been used in many applications such as an insulator of electric devices, a support in catalysis, and a substrate for thin film depositions [1–4]. Due to its importance, material properties of MgO, such as grain growth behavior, diffusion behavior, grain boundary structure, surface structure, and so on, have been investigated experimentally and theoretically so far [5–8]. In addition to those properties, the defect formation behaviors in the rock salt-type oxides have been investigated because they affect the electric properties and the atomic migration behaviors of rock salt-type oxides. To investigate the defect formation behaviors in the rock salt-type oxides, theoretical calculations using a first principles method and an empirical potential method have been used [8–12]. Especially, using the first principles method, the dependence of the defect energetics on atmospheres and Fermi energy, which are both important factors in actual applications, can be discussed. Thus, to obtain comprehensive information on the defect energetics in the rock-salt type oxides, use of the first principles calculation is important. On the other hand, although first principles calculations of the defect energetics in MgO have been reported by some groups, reports on other rock salt-type oxides, such as CaO, SrO, and BaO, are very limited.

In this study, the oxygen vacancy formation energies in four types of rock salt-type oxides, MgO, CaO, SrO, and BaO, were systematically investigated using a first-principles projector augmented wave (PAW) method based on a density functional theory (DFT), and the vacancy formation behaviors in those rock salt-type oxides were compared with each other. In the present study, the calculation error derived from a finite-size cell interaction was corrected by the method proposed by Makov and Payne [13]. This finite-size correction is known to be important to investigate the defect energetics of functional

*Corresponding author.
*E-mail address:* teru@iis.u-tokyo.ac.jp (T. Mizoguchi).

0272-8842/$ - see front matter © 2012 Elsevier Ltd and Techna Group S.r.l. All rights reserved.
http://dx.doi.org/10.1016/j.ceramint.2012.10.079

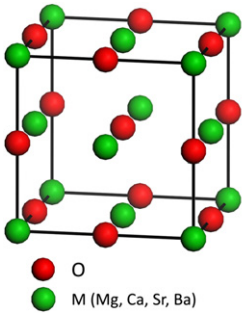


| a(Å) | Exp. | Calc. |
|---|---|---|
| MgO | 4.21 | 4.26 |
| CaO | 4.81 | 4.83 |
| SrO | 5.16 | 5.20 |
| BaO | 5.54 | 5.61 |

Fig. 1. Schematic view of unit cell of rock salt-type oxides, and experimental and calculated lattice constants of MO (M: Mg, Ca, Sr, and Ba).

materials [14–16]. In this study, the finite-size cell dependences were investigated by calculating with various sizes of supercells up to 512 atoms. In addition, the band gap correction for a neutral oxygen vacancy, which is also important for the calculation of wide gap materials, was also performed. Through this study, the formation energies of neutral and charged oxygen vacancies in MgO, CaO, SrO, and BaO were systematically investigated.

## 2. Methodology

First-principles PAW calculations with the Perdew–Burke–Ernzerhof (PBE) generalized gradient approximation (GGA) functional were performed using the VASP code [17–19]. A plane-wave cut off energy ($E_{cut}$) of 500 eV was used. For oxygen, $2s^2$ and $2p^4$ electrons were considered as valence electrons, while $2p^6$ and $3s^2$ for Mg, $3p^6$ and $4s^2$ for Ca, $4s^2$, $4p^6$ and $5s^2$ for Sr, and $5s^2$, $5p^6$ and $6s^2$ for Ba were considered as valence electrons, respectively. Fig. 1 shows schematic structure of a unit cell of the rock salt-type oxides.

Before going to the supercell calculations for the vacancies, calculations of the perfect MO were carried out. The primitive cells were calculated using $24 \times 24 \times 24$ $k$-point mesh generated by the Monkhorst–Pack scheme (1300 irreducible $k$-points) [20]. Calculated and experimental lattice constants are shown in Fig. 1. It is found that the optimized lattice parameters are in good agreement with the experimental and previously reported theoretical values (Fig. 1) [21–24]. Based on the optimized structure of the perfect MO, the primitive cells and unit cells were expanded to make large supercells for the vacancy calculations.

To introduce an isolated oxygen vacancy, an interior oxygen atom was removed from the supercells. In order to take account of atomistic relaxation around the vacancy, all atoms in the supercells were allowed to be relaxed until the residual force becomes less than 0.05 eV/Å under the fixed volume condition. In the supercell calculations, numerical integrations over the Brillouin zone were performed at the Γ-point for every size of the supercells.

The formation energies of the vacancies in MO were calculated from total energies of the supercells, based on the standard formalism by Zhang and Northrup [25]. For compound systems, formation energies of vacancies depend on the atomic chemical potentials of atoms and the electron chemical potential i.e., Fermi energy. For a vacancy with a charge state $q$, the formation energy is given by

$$E_T = E_T(\text{defect} : q) - \{E_T(\text{perfect}) - \boldsymbol{\mu}_O\} + n(\boldsymbol{\varepsilon}_F + E_{VBM})$$

where $E_T$(defect:$q$) and $E_T$(perfect) are the total energy of the supercell containing an oxygen vacancy in a charged state $q$ and that of the perfect supercell, respectively. $n_O$ is the number of oxygen atoms removed from the perfect supercell to introduce isolated vacancies. $\mu_O$ is the atomic chemical potential of oxygen, and $\varepsilon_F$ is the Fermi energy measured from valence band maximum (VBM) [26]. For each vacancy species, its charge state $q$, varying from neutral to fully ionized, was considered, namely 0 and +2 for an oxygen vacancy. For charged defects, the total charge of supercells was neutralized by using background charge.

The formation energies of vacancies in MO also depend on the chemical potentials of the oxygen atom. The chemical potential of oxygen was determined from the equilibrium conditions of the phases containing M and oxygen. In order to consider the chemical potentials, the first-principles calculations were performed for primitive structure of each element. Then chemical potentials could be defined as

$$\boldsymbol{\mu}_O(O\text{-rich}) = \boldsymbol{\mu}_O(O \text{ primitive cell}),$$

$$\boldsymbol{\mu}_O(M\text{-rich}) = \boldsymbol{\mu}_{MO} - \boldsymbol{\mu}_M(M \text{ primitive cell}).$$

The Fermi level $\varepsilon_F$ was varied within the band gap. The calculated band gap was found to be 4.37 eV for MgO, 3.53 eV for CaO, 3.17 eV for SrO and 1.98 eV for BaO, by calculating the total energies of the charged and neutral cells. This value is lower than the experimental values of 7.6 eV for MgO, 6.9 eV for CaO, 6.4 eV for SrO, and 4.4 eV for BaO [27,28]. This difference between the calculated and experimental band gaps is hereafter called $\Delta E_g$. By the presence of the oxygen vacancy, the vacancy state is usually generated below the conduction band minimum (CBM), and extra electrons are introduced to the vacancy state. Thus, this band gap error in the calculation often influences the formation energy of the neutral oxygen vacancy. To correct this band gap error, the formation energy of a neutral oxygen vacancy was adjusted to be the sum of the calculated value and $\Delta E_g$ multiplied by the number of electrons $m$ at the donor levels, so that the $m$ is 2 in the case of present study.

In addition, finite-cell size correction was also performed in this study. In the supercell calculation of the charged vacancies using periodic boundary conditions, Coulomb interactions are noted between the charged vacancy and anticlastic background charge, so called jellium, depending on the size of the supercells. It is necessary to correct this spurious interaction of charged vacancies to evaluate their formation energies. Errors in the defect formation energies due to the spurious electrostatic interaction in the finite-sized cells were corrected using the scheme proposed by

Leslie and Gillan [29], and by Makov and Payne [13]. It assumes that the interactions between the multipoles at the defect site, and those between the multipoles and the jellium background, lead to $L^{-1}$, $L^{-3}$, and $L^{-5}$ dependences of the formation energies (where $L$ is the average interdefect distance). The $L^{-1}$ term corresponds to the Madelung energy for an array of point charges $q_c$ in an effective medium with a static dielectric constant, $\varepsilon_0$, $E_c=\alpha q_c^2/2\varepsilon_0 L$, where $\alpha$ is the appropriate Madelung constant. This term is considered to be dominant for the charged defects in the ionic crystals. In this study, the various sizes of supercells were constructed by repeating the optimized primitive cell that contains 2 atoms by $3\times3\times3$, $4\times4\times4$, and $5\times5\times5$, and the unit cell that contains 8 atoms by $2\times2\times2$, $3\times3\times3$, and $4\times4\times4$ in the $x$, $y$, and $z$ directions, so that rhombohedral supercells containing 54, 128, and 250 atoms and cubic supercells containing 64, 216, and 512 atoms were employed for this finite-size cell correction. In the same manner, vacancy formation energies have been investigated so far, and they have successfully reproduced and explained the vacancy formation behaviors in many ceramic materials [12–16,29–35].

## 3. Results and discussion

Results for the finite-size correction for $V_O$ with neutral and charged states are shown in Fig. 2. In this figure, oxygen-rich atmosphere was considered and $\varepsilon_f$ was set to half of the experimental band gap. For charged defects, it is found that the formation energies showed almost linear $L^{-1}$ dependences as proposed by Leslie and Gillan [29], and Makov and Payne [13]. This demonstrates the appropriateness of the correction model and that the formation energies can be extrapolated to the dilute (infinite cell-size) limit using the $L^{-1}$ dependences obtained by a linear fit. Corrected values of the charged O vacancy formation energies under the above condition are 10.3 eV for MgO, 10.1 eV for CaO, 9.1 eV for SrO, and 7.2 eV for BaO.

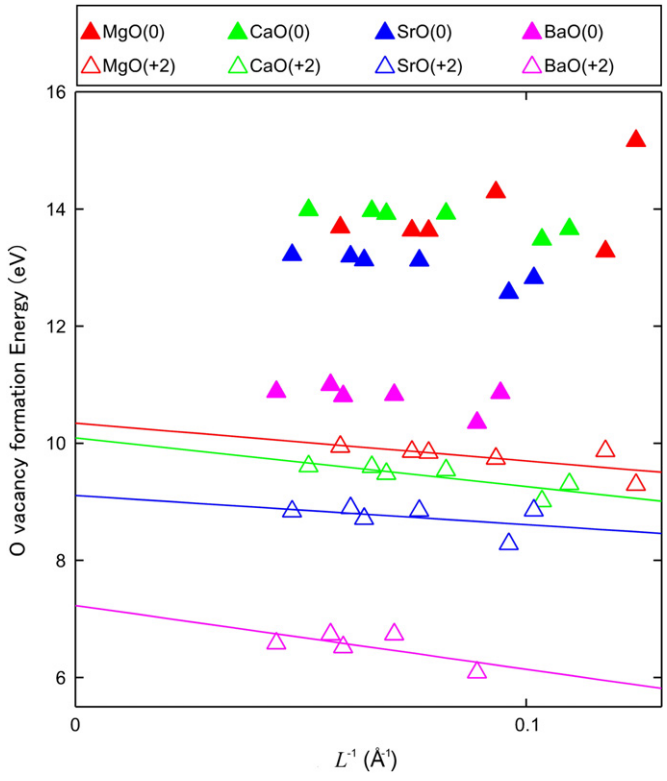


Fig. 2. Formation energies of O vacancy in the neutral and charged states as a function of $L^{-1}$ (where $L$ is the average interdefect distance).

In the case of the neutral vacancies, it is found that the dependence on the supercell size is basically very small in the range of large supercells. However, it is clearly found that the formation energy of the neutral oxygen vacancy is largely deviated in the smaller supercells, such as 54 and 128 atoms. This indicates that the supercells around 100 atoms are not enough to describe the defect energetics in those rock salt-type oxides. From this result, it was found that the finite-size effects in both neutral and charged oxygen vacancies are not so significant when several hundred atom supercells were employed. Thus, the results obtained by using 512 atom supercells were hereafter used.

Fig. 3 shows the dependence of vacancy formation energy on Fermi energy at the oxygen-rich limits. The range of the Fermi energy was set from VBM = 0 eV to the experimental band gap energies. Defect level induced by the oxygen vacancy could be described as a cross point of the charged and neutral lines. For each case, the charged states that are energetically favorable at a given Fermi energy are plotted as a solid line. In all MO, the defect levels induced by the oxygen vacancy are basically located below the CBM, and the vacancy states for MgO, CaO, SrO, and BaO are placed 1.97 eV, 1.28 eV, 1.02 eV, and 0.06 eV below the CBM respectively, indicating that the neutral oxygen vacancy in BaO has potential to act as a donor, whereas that in MgO cannot be an effective donor.

Dependence of the oxygen vacancy formation energy on the oxygen chemical potential is shown in Fig. 4. $\mu_O$ at the oxygen-rich condition was set to 0 eV and $\mu_O$ at the metal (M)-rich condition corresponds to the terminal points of plotted lines. Only the result of the neutral oxygen vacancy is shown because the charged vacancy shows similar tendency. From Fig. 4, it is commonly found that the oxygen vacancies in MOs are preferably formed in the reduction atmosphere (lower $\mu_O$), whereas it is unfavorable in the oxidization atmosphere. In addition, it is also found that vacancy formation energies in MgO, CaO, and SrO are basically similar to each other, around 7.5 eV under the reduction atmosphere and 13–14 eV under the oxidization atmosphere, whereas BaO shows lower oxygen vacancy formation energy than other compounds, around 5.5 eV under the reduction atmosphere and 11 eV under the oxidization atmosphere. This result indicates that the oxygen vacancy is more abundant in BaO than in MgO, CaO, and SrO.

In order to discuss the reason why BaO shows lower oxygen vacancy formation energy, atomic displacements induced by the vacancy formation and the band gaps of

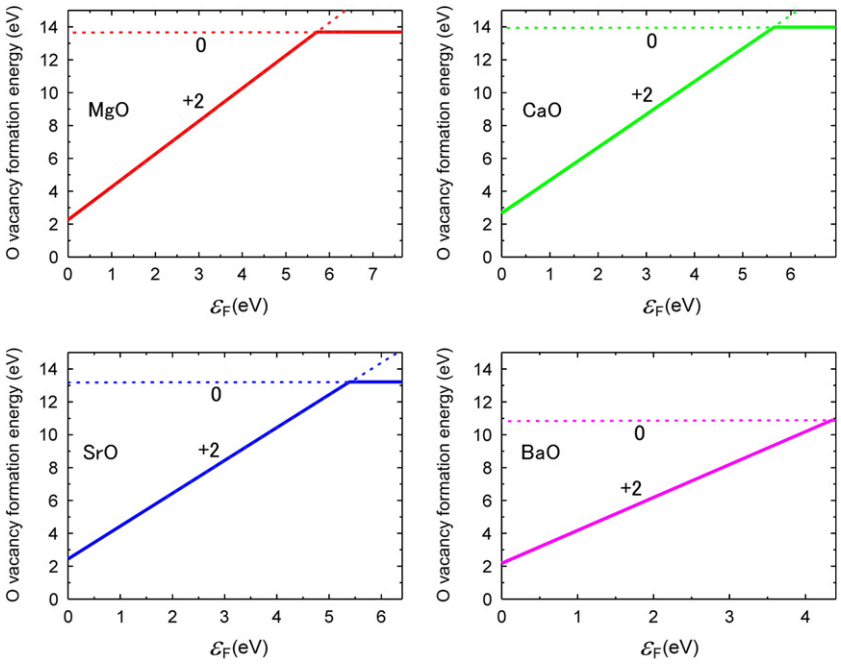


Fig. 3. Formation energies of O vacancy in the neutral and charged states as a function of Fermi energy, $\varepsilon_F$, where $\varepsilon_F$ was set to 0 at the energy of VBM. The supercell size is 512 atoms and the energies are for the oxidization limit.

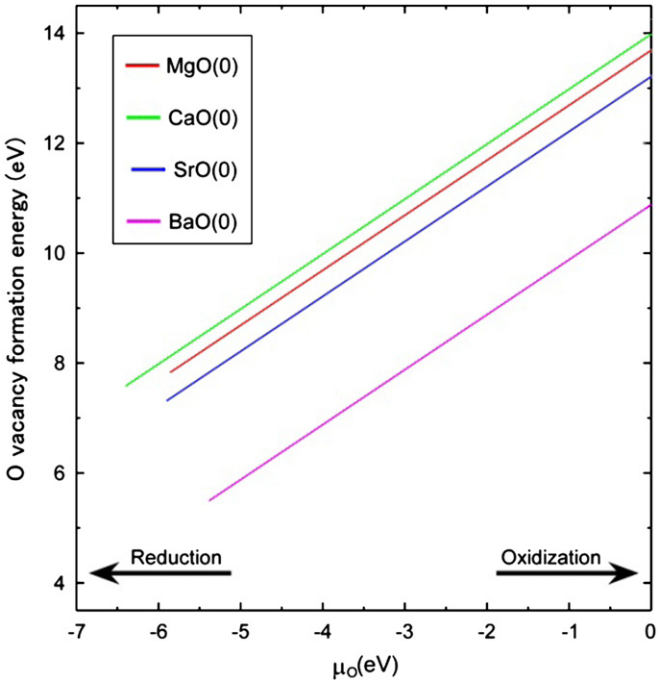


Fig. 4. Formation energies of O vacancy in the neutral states as a function of O chemical potential, $\mu_O$, where $\mu_O$ was set to 0 at the O-rich limit.

those compounds were compared, because it has been reported that those values are related to the vacancy formation energies [10,12,31]. This analysis was performed by using 512 atom supercells with the charged vacancy under the oxidization atmosphere and the Fermi energy was set to half of the experimental band gap, but other calculation conditions show the same results. Fig. 5(a) shows the oxygen vacancy formation energies as a function of the magnitude of atomic displacements induced by the oxygen vacancy. The absolute values of the atomic displacements were summed up for all atoms in the supercell and then divided by the number of atoms in the supercell. Although the values are a little deviated, it is seen that MgO, CaO, and SrO, which show larger vacancy formation energy, have smaller atomic displacements, whereas larger atomic displacements are induced in BaO that shows smaller formation energy (Fig. 5(a)). This relationship between the vacancy formation energy and the atomic displacements is consistent with that in a previous report [31].

Another trend of vacancy formation energy and band gap is confirmed in Fig. 5(b) where the calculated oxygen vacancy formation energy is plotted as a function of the experimental band gap energy. There is a very clear trend that large band gap materials, MgO, CaO, and SrO, show larger formation energies and the small band gap material, BaO, requires smaller formation energy. This relation is consistent with those in previous studies [10,12].

From this analysis, it can be concluded that the smaller vacancy formation energy in BaO is caused by the larger atomic displacements induced by the oxygen vacancy and the smaller band gap.

## 4. Summary

In conclusion, we performed the first-principles projector augmented wave calculations of oxygen vacancy energetics in rock salt-type oxides MO (M: Mg, Ca, Sr, and Ba). Examining various sizes of supercells, from 54 to 512 atoms, it was found that the calculation with sufficiently large supercells is indispensable to describe the

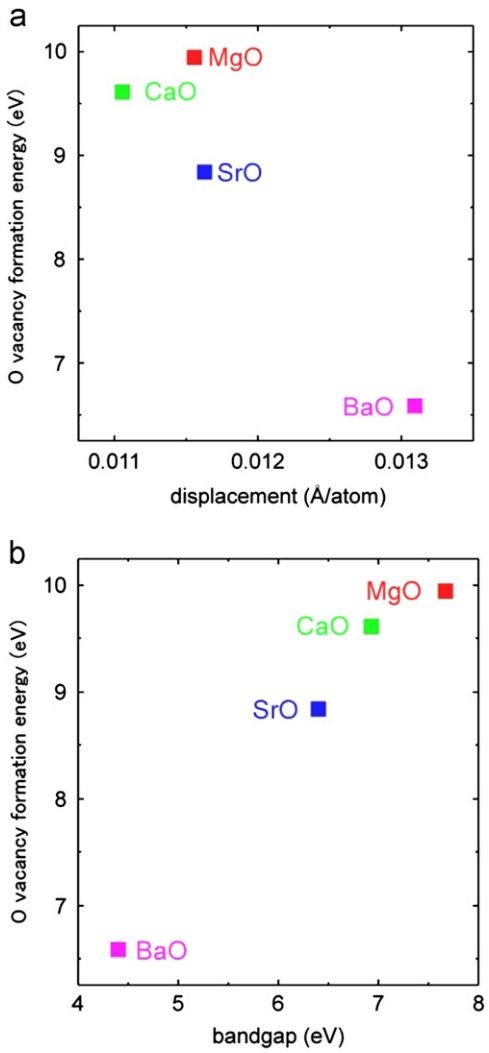


Fig. 5. (a) Formation energies of O vacancy in the charged states as a function of average displacement obtained after lattice relaxation calculation and (b) formation energies of O vacancy in the charged states as a function of experimental bandgap energy of each material.

defect formation energetics of those rock salt-type oxides. It was found that the oxygen vacancy formation energy in BaO is lower than those in the other rock salt-type oxides, while those in MgO, CaO, and SrO are similar to each other. The vacancy state induced by the oxygen vacancy is deep in MgO and it becomes closer to CBM in CaO, SrO, and BaO in that order. From detailed investigations, it was concluded that the smaller vacancy formation energy in BaO is caused by the larger atomic displacements induced by the vacancy formation and the smaller band gap.

## Acknowledgments

This study was supported by a Grant-in-Aid for Scientific Research (Nos. 22686059 and 23656395) from the Ministry of Education, Culture, Sports, Science, and Technology (MEXT) of Japan. Some calculations were performed by the supercomputing system in ISSP, University of Tokyo.

## References

[1] H.W. Choi, S.Y. Kim, W.K. Kim, J.L. Lee, Enhancement of electron injection in inverted top-emitting organic light-emitting diodes using an insulating magnesium oxide buffer layer, Applied Physics Letters 87 (2005) 082102.
[2] M. Haruta, Size- and support-dependency in the catalysis of gold, Catalysis Today 36 (1997) 153.
[3] T. Katase, Y. Ishimaru, A. Tsukamoto, H. Hiramatsu, T. Kamiya, K. Tanabe, H. Hosono, Advantageous grain boundaries in iron pnictide superconductors, Nature Communications 2 (2011) 409.
[4] T. Tohei, T. Mizoguchi, H. Hiramatsu, H. Hosono, Y. Ikuhara, Interface atomic structure of LaCuOSe:Mg epitaxial thin film and MgO substrate, Materials Science and Engineering B 173 (2010) 229–233.
[5] Y.M. Chiang, A.G. Henriksen, D. Finello, W.D. Kingery, Characterization of grain–boundary segregation in MgO, Journal of the American Ceramic Society 64 (1981) 383.
[6] J. Carrasco, N. Lopez, F. Illas, H.J. Freund, Bulk and surface oxygen vacancy formation and diffusion in single crystals, ultrathin films, and metal grown oxide structures, Journal of Chemical Physics 125 (2006) 074711.
[7] J. Rubio, H.T. Tohver, Y. Chen, M.M. Abraham, Trapped-hole defects in SrO, Physical Review B 14 (1976) 5466.
[8] C.D. Valentin, R. Ferullo, R. Binda, Gianfranco Pacchioni, Oxygen vacancies and peroxo groups on regular and low-coordinated sites of MgO, CaO, SrO, and BaO surfaces, Surface Science 600 (2006) 1147–1154.
[9] J. Osorio-Guillén, S. Lany, S.V. Barabash, A. Zunger, Magnetism without magnetic ions: percolation, exchange, and formation energies of magnetism-promoting intrinsic defects in Ca, Physical Review Letters 96 (2006) 107203.
[10] I. Tanaka, F. Oba, K. Tatsumi, M. Kunitsu, M. Nakano, H. Adachi, Theoretical formation energy of oxygen-vacancies in oxides, Materials Transactions 43 (2002) 1426–1429.
[11] D.D. Richardson, A calculation of vacancy formation energies in strontium oxide, Physica Status Solidi 106 (1981) 223–227.
[12] I. Tanaka, K. Tatsumi, M. Nakano, H. Adachi, F. Oba, First-principles calculations of anion-vacancies in oxides and nitrides, Journal of the American Ceramic Society 85 (2002) 68–74.
[13] G. Makov, M.C. Payne, Periodic boundary conditions in ab initio calculations, Physical Review B 51 (1995) 4014.
[14] F. Oba, A. Togo, I. Tanaka, Defect energetics in ZnO: a hybrid Hartree–Fock density functional study, Physical Review B 77 (2008) 245202.
[15] C.W.M. Castleton, S. Mirbt, Finite-size scaling as a cure for supercell approximation errors in calculations of neutral native defects in InP, Physical Review B 70 (2004) 195202.
[16] T. Yamamoto, T. Mizoguchi, http://dx.doi.org/10.1103/PhysRevB.00.004100, in press.
[17] J.P. Perdew, K. Burke, M. Ernzerhof, Generalized gradient approximation made simple, Physical Review Letters 78 (1996) 18–3865.
[18] J.P. Perdew, K. Burke, M. Ernzerhof, Generalized gradient approximation made simple, Physical Review Letters 78(7) 1997 1396.
[19] G. Kresse, Ph.D. Thesis, Technische Universitat, Wien, 1993.
[20] H.J. Monkhorst, J.D. Pack, On special points for Brillouin zone integrations, Physical Review B 13 (1976) 5188.
[21] B.J. Skinner, The thermal expansion of thoria, periclase and diamond, American Mineralogist 42 (1957) 39–55.
[22] D.J.M. Bevan, F.J. Lincoln, F.D. Richardson, A study of the non-stoicheiometric, lime-type phase occurring in the system Ca–O–N, Australian Journal of Chemistry 19 (1966) 725–732.
[23] G. Brauer, N. Schultz, Die mischkristallreihe EuO–SrO und ein-neuesverfahrenzurdarstellung von euo, Journal of the Less-Common Metals 13 (1967) 213–218.
[24] R.J. Zollweg, X-ray lattice constant of barium oxide, Physical Review 100 (1955) 671–673.

[25] S.B. Zhang, J.E. Northrup, Chemical potential dependence of defect formation energies in GaAs: application to Ga self-diffusion, Physical Review Letters 67 (1991) 2339.
[26] D.B. Laks, C.G. Van de Walle, G.F. Neumark, P.E. Blöchl, S.T. Pantelides, Native defects and self-compensation in ZnSe, Physical Review B 45 (1992) 10965.
[27] R.C. Whited, C.J. Flaten, W.C. Walker, Exciton thermoreflectance of MgO and CaO, Solid State Communications 13 (1973) 1903.
[28] F. Tran, P. Blaha, Accurate band gaps of semiconductors and insulators with a semilocal exchange-correlation potential, Physical Review Letters 102 (2009) 226401.
[29] M. Leslie, M.J. Gillan, The energy and elastic dipole tensor of defects in ionic crystals calculated by the supercell method, Solid State Physics 18 (1985) 973–982.
[30] H.S. Lee, T. Mizoguchi, T. Yamamoto, S.J.L. Kang, Y. Ikuhara, First-principles calculation of defect energetics in cubic-$BaTiO_3$ and a comparison with $SrTiO_3$, Acta Materialia 55 (2007) 6535.
[31] M. Imaeda, T. Mizoguchi, Y. Sato, H.S. Lee, S.D. Findlay, N. Shibata, T. Yamamoto, Y. Ikuhara, Atomic structure, electronic structure, and defect energetics in [001](310) Σ5 grain boundaries of $SrTiO_3$ and $BaTiO_3$, Physical Review B 78 (2008) 245320.
[32] H.S. Lee, T. Mizoguchi, J. Mitsui, T. Yamamoto, S.J.L. Kang, Y. Ikuhara, Defect energetics in $SrTiO_3$ symmetric tilt grain boundaries, Physical Review B 83 (2011) 104110.
[33] T. Mizoguchi, H. Ohta, HS. Lee, N. Takahashi, Y. Ikuhara, Controlling interface intermixing and property of SrTiO3 based superlattices, Adv. Funct. Mater. 21 (2011) 2258–2263.
[34] H.S. Lee, T. Mizoguchi, T. Yamamoto, Y. Ikuhara, First principles study on intrinsic vacancies in cubic and orthorhombic $CaTiO_3$, Materials Transactions 50 (2009) 977.
[35] T. Mizoguchi, Study on Atomic and Electronic Structures of Ceramic Materials using Spectroscopy, Microscopy, and First Principles Calculation, Journal of Ceramics Society of Japan 119 (2011) 325–333.